

ARTICLE OPEN



Sumoylated SnoN interacts with HDAC1 and p300/CBP to regulate EMT-associated phenotypes in mammary organoids

Ayan Chanda¹, Anusi Sarkar¹, Lili Deng¹, Azad Bonni² and Shirin Bonni¹✉

© The Author(s) 2023

Protein post-translational modification by the small ubiquitin-like modifier (SUMO) regulates the stability, subcellular localization, and interactions of protein substrates with consequences on cellular responses including epithelial-mesenchymal transition (EMT). Transforming growth factor beta (TGFβ) is a potent inducer of EMT with implications for cancer invasion and metastasis. The transcriptional coregulator SnoN suppresses TGFβ-induced EMT-associated responses in a sumoylation-dependent manner, but the underlying mechanisms have remained largely unknown. Here, we find that sumoylation promotes the interaction of SnoN with the epigenetic regulators histone deacetylase 1 (HDAC1) and histone acetylase p300 in epithelial cells. In gain and loss of function studies, HDAC1 suppresses, whereas p300 promotes, TGFβ-induced morphogenetic changes associated with EMT-related events in three-dimensional multicellular organoids derived from mammary epithelial cells or carcinomas. These findings suggest that sumoylated SnoN acts via the regulation of histone acetylation to modulate EMT-related effects in breast cell organoids. Our study may facilitate the discovery of new biomarkers and therapeutics in breast cancer and other epithelial cell-derived cancers.

Cell Death and Disease (2023)14:405; <https://doi.org/10.1038/s41419-023-05921-x>

INTRODUCTION

Epithelial-mesenchymal transition (EMT) is a fundamental cellular process that is critical for multicellular organism development and homeostasis [1]. EMT also regulates cellular activity in diseased states including organ fibrosis and cancer [2]. During EMT, epithelial cells transdifferentiate to form less adherent and more motile mesenchymal cells via a complex cell-signaling network [3–5]. One of the major regulators of EMT is the transforming growth factor beta (TGFβ) signaling pathway [1, 6, 7]. Thus, identifying and characterizing novel regulators of TGFβ-induced EMT is a subject of intense interest in biology.

The canonical Smad pathway plays a major role in mediating TGFβ signaling from the cell surface to the nucleus. TGFβ triggers the assembly of an active transmembrane type I and II receptor ser/thr kinase complex that induces the phosphorylation of the Receptor-regulated Smads (R-Smad), Smad 2 and 3 [8, 9]. The phosphorylated Smad 2 and 3 (pSmad2/3) bind Smad4, the common partner Smad, and the complex accumulates in the nucleus, where it binds to specific DNA elements on TGFβ-target genes and in conjunction with diverse transcription factors and transcriptional coregulators controls the expression of a wide array of TGFβ-responsive gene in a cell- and context-specific manner that manifests as different responses including regulation of cell plasticity, e.g., EMT [10, 11].

The Ski-related novel protein N (SnoN) is a key component of the TGFβ signaling pathway [12–15]. SnoN can positively or negatively regulate TGFβ-signaling with consequences for biological responses [16, 17]. SnoN forms a complex with Smad2, Smad3, and Smad4 [18, 19]. Initial studies proposed a model

whereby the closely related protein Ski leads to the dissociation of Smad2/3-Smad4 complex and thus suppresses TGFβ signaling [20]. In contrast, recent studies suggest that SnoN can form a ternary complex with and stabilizes the Smad2/3-Smad4 multi-protein complex [19]. SnoN associates with other proteins including chromatin remodelers such as histone deacetylases (HDACs) and histone acetyl transferases (HATs), which are recruited to promoters and enhancers of TGFβ responsive genes [15, 21]. How SnoN functions in modulating TGFβ signaling is regulated is an important question.

Sumoylation is a post-translational modification in which the protein small ubiquitin like modified (SUMO) is covalently conjugated to specific lysine residues in target proteins [22]. Sumoylation regulates target protein stability, localization and interaction with other proteins [22, 23]. Interestingly, SnoN is a SUMO target and Lysines 50 and 383, which reside within SUMO consensus motifs, are sites of sumoylation in SnoN. PIAS1 and TIF1γ represent two distinct SUMO E3 ligases that promote the sumoylation of SnoN [14, 24, 25]. Importantly, sumoylated SnoN mediates the ability of PIAS1 and TIF1γ to suppress TGFβ-induced EMT-related effects in epithelial cells and carcinoma-derived sheets and organoid cultures [24–26]. However, the downstream mechanisms by which sumoylated SnoN suppresses TGFβ-induced EMT had remained to be identified.

In this study, we find that sumoylation enhances SnoN association with the histone deacetylase HDAC1 and histone acetylase p300. Whereas HDAC1 suppresses, p300 promotes TGFβ-induced EMT-associated phenotypic changes in three-dimensional organoids derived from mammary epithelial cells or

¹Department of Biochemistry and Molecular Biology, Arnie Charbonneau Cancer Institute, Cumming School of Medicine, University of Calgary, Calgary, Canada. ²Neuroscience and Rare Diseases, Roche Pharma Research and Early Development (pRED), Roche Innovation Center Basel, Basel, Switzerland. ✉email: sbonni@ucalgary.ca
Edited by Angelo Peschiaroli

Received: 18 August 2022 Revised: 14 June 2023 Accepted: 22 June 2023
Published online: 07 July 2023

carcinomas. Our findings suggest that sumoylated SnoN suppresses EMT-associated responses by regulating histone acetylation in mammary cell-derived organoids.

METHODS

Plasmids

To establish mammalian cells stably expressing SnoN, a pCaGip vector containing a cDNA to express a puromycin resistance marker was employed to generate constructs containing cDNA encoding wild type SnoN, a SUMO loss-of-function SnoNKdR, or a SUMO gain-of-function stable fusion SUMO-SnoN protein. The puromycin resistance marker and the SnoN proteins are encoded by a bicistronic transcript containing Internal Ribosomal Entry Site (IRES) as part of the pCaGip vector [25].

The pBJ5 vector containing SR α promoter, comprising the simian virus 40 early promoter and the R-U5 segment of human T-cell leukemia virus type 1 long terminal repeat, and cDNA encoding the C-terminally FLAG-tagged histone deacetylase 1 (HDAC1/FLAG) protein, is a gift from Wen-Ming Yang, Moffitt Cancer Center, USA [27]. CMV-based plasmid containing cDNA encoding the C-terminally hemagglutinin tagged p300 (p300/HA) protein, and a U6-based plasmid encoding an shRNA targeting the human and mouse p300 (p300i) are described [16].

Renilla Luciferase (RLuc) tagged-SnoN (Rluc/SnoN) expression vector is described [28]. SnoNKdR insert from the pCMV5B/MYC/SnoNKdR plasmid was subcloned using Sall and XbaI (NEB, Canada) digestion into Sall- and XbaI-digested pCMV5B/RLuc/SnoN backbone.

SUMO-SnoN insert was PCR-amplified from pCMV5B/SUMO-SnoN plasmid using the following primers: Forward Primer: 5' AGGCCTCGAGG ATCTGACCGAGGAGCCAAAC 3', and Reverse Primers: 5' CAAACTGGGATTT AAATGCAAAG 3'. The insert was digested using XhoI and SwaI (NEB, Canada) and subcloned into Sall- and SwaI-digested pCMV5B/RLuc/SnoN backbone to generate pCMV5B/RLuc/SUMO-SnoN.

The pBJ5/HDAC1/FLAG was used as a template to PCR amplify a fragment of HDAC1 flanked by SacII (NEB, Canada) and NdeI (NEB, Canada) restriction endonuclease cut sites. The following primers were used: Forward Primer: 5' CTAGAGCGGCCGCGGATCCGCCATGGCGAGAC 3', and Reverse Primer: 5' GTCTCATATGTCCAGCACCGGGCAACGTTACGAA TGGTGT GACCACCGCCTC 3'. The underlined and bold face nucleotide (G) in the reverse is to amplify HDAC1 in which Tyrosine 303 is converted to histidine (H) to generate a deacetylase inactive HDAC1 expression construct [29]. The PCR fragment was digested with and ligated with SacII and NdeI-digested pBJ5/HDAC1/FLAG vector to generate pBJ5/HDAC1YH/FLAG expressing vector.

HDAC1 RNA interference (HDAC1i) construct was generated in pU6/EGFP vector containing DNA encoding shRNAs against HDAC1 under the U6 promoter, and the green fluorescent protein (GFP) under CMV promoter. HDAC1i, targeting nucleotides 735–757 in exon 8 of human HDAC1, and corresponding regions in mouse and rat HDAC1, was generated using the following primer pair:

Forward Primer: 5' GTCCAAAGTAATGGAGATGTTCCCAAGTTAACGGAA CATCTCCATTACTTTGGACTTTTTG 3' and Reverse Primer: 5' AATCAAAA GTCCAAAGTA ATGGAGATGTTCCGTTAACTTGGGAACATCTCCATTACTTTGAC 3'.

All constructs were confirmed by sequencing.

Cell lines, transfections, and reagents

The human embryonic kidney 293T (HEK293T) epithelial cells, human MDA-MB-231 breast cancer cells, and NAMRU murine mammary gland (NMuMG) epithelial cells (source the American Type Culture Collection (ATCC), USA) were cultured in Dulbecco's modified Eagle's medium (DMEM) with high glucose and L-glutamine (Invitrogen, Canada) supplemented with 10% fetal bovine serum (FBS; Invitrogen, Canada). A total of 10 mg/ml recombinant human insulin (Invitrogen, Canada) was also added in the case of the NMuMG cells. In total 2 μ g/ml puromycin was used in appropriate media to culture stable expression cell lines. Cells were maintained in a humidified incubator at 37 °C in 95% air and 5% CO₂. All cell types were confirmed to be free of pathogenic Mycoplasma strains by a PCR-ELISA kit (Lonza, Switzerland).

HEK293T cells were transfected by the calcium-phosphate precipitation method [30]. The MDA-MB-231 and NMuMG cells were transfected using Lipofectamine 3000 reagent (Invitrogen, Canada) as per the manufacturer's instructions [25, 26, 31].

Lyophilized recombinant human homodimerized mature transforming growth factor beta 1 (TGF β 1) (R&D systems, USA), referred to as TGF β throughout the manuscript, was reconstituted in 30% acetonitrile and 0.01% trifluoroacetic acid at a stock concentration of 10 μ M, divided into several 2 μ L aliquots in 200 μ L microfuge tubes, and stored at –80 °C. The TGF β stock solution was then serially diluted to a final concentration of 100 pM in growth medium in 3D and 2D cell cultures. SB431542 (Millipore-Sigma, Canada), referred to as KI in this manuscript, is a small molecule selective inhibitor of the TGF β type I receptor kinase, also known as ALK5, was reconstituted in dimethyl sulfoxide (DMSO) (Millipore-Sigma, Canada) as a 10 mM stock solution, which was used to obtain 10 μ M final concentration in growth medium in organoid cultures as indicated.

Immunoprecipitation and immunoblotting assays

Cells were seeded to achieve approximately a 30% confluency on the next day, when they were transfected with appropriate plasmids. Two days post-transfection, cells were lysed in TNTE (50 mM Tris, 150 mM NaCl, 0.5% [v/v] Triton X-100 and 1 mM EDTA) buffer-containing protease inhibitors and phosphatase inhibitors [25, 26, 31]. Cellular extracts were centrifuged at 14000 \times g for 10 minutes at 4 °C. 95% of the supernatant was used for immunoprecipitation (IP) using appropriate antibodies and 5% was saved for protein determination and input sample analysis. The immunocomplexes and input lysates were subjected sodium dodecyl sulfate polyacrylamide gel electrophoresis (SDS-PAGE) to resolve the protein contents followed by transfer to nitrocellulose (NC) membranes [24, 25, 31]. The NC membranes were incubated with mouse anti-FLAG, mouse anti-HA, mouse anti-GFP (Santa Cruz, Canada), rabbit anti-SnoN (Proteintech, USA), rabbit anti-HDAC1 (Santa Cruz, Canada), mouse anti-p300 (Santa Cruz, Canada), rabbit anti-phospho-Smad2 (Abcam, USA), mouse anti-Smad2/3 (BD Transduction Laboratories, USA), or mouse anti-actin (Santa Cruz, Canada), as the primary antibody, and HRP-conjugated goat anti-mouse (Millipore Sigma, Canada) or donkey anti-rabbit IgG (VWR, Canada) as the secondary antibody. Immunocomplexes (80%) and input lysate (10–15%) from cells expressing RLuc alone or in fusion with SnoN were subjected to Renilla luciferase assays using the Renilla luciferase kit (Promega, USA) and the Orion II luminometer (Berthold Detection Systems, Germany) detection system. Prior to RLuc analysis, immunocomplexes were resuspended in TNE buffer-containing 0.1% Triton X-100 [28].

Three-dimensional cultures

Three-dimensional cultures of cells were prepared in ultra-low attachment plates (8-well chamber slides (Millicell EZ Slide, Millipore) or 96-well flat-bottom, (BD Biosciences, ON, Canada)). Each well of the 8-well chamber slides and the 96-well dish were precoated with 75 and 50 μ L, respectively, of 3 mg/mL Matrigel (BD Biosciences, Canada)-containing antibiotic-antimycotic-growth medium and incubated for 1 h in a tissue culture hood at 37 °C and 5% CO₂ to allow formation of the Matrigel bed/cushion. Next, 75 μ L or 50 μ L of isolated cells resuspensions in 5 mg/ml Matrigel in growth medium, at a concentration of 10 cells/ μ L (NMuMG cells) and 6 cells/ μ L (MDA-MB-231 cells), were layered on top of the Matrigel cushion in each well of the 8-well chamber slide or 96-well dish, respectively, and incubated for 1 h at 37 °C and 5% CO₂ to allow the upper Matrigel-cell layer to solidify. A total of 50 μ L of complete medium was then carefully added to the Matrigel-cell layer. The 3D-cell cultures received specific treatments on the next and every third day for a total of 8 days of culturing. Differential interference contrast (DIC) images of six representative organoids from each well were captured using a microscope (Olympus IX70) using a 30 \times objective, after overall estimation and phenotype assessment of the total number of organoids per well (acini vs. filled for NMuMG organoids, non-deformed/spherical vs. deformed for NMuMG and MDA-MB-231 organoids) [24, 26, 31–34]. NMuMG and MDA-MB-231 cell-derived multicellular structures were assessed for hollow centered- (30–40 μ m in diameter) and filled- spheres appearances, respectively. In addition, multicellular structures with shapes deviating from the outer round-smooth-surfaced phenotype, predominantly observed in vector-control cells, were quantified, and referred to as "deformed". Deformed phenotypes included organoids showing invagination/budding and/or basal-surface single cell invasiveness into the matrix. In the case of NMuMG cell-derived multicellular structures, deformed multicellular structures also included filled-lumen organoids with greater than 100 μ m diameter. Each experiment was repeated at least three independent times for statistical inference.

Immunofluorescence and fluorescence cell-based analyses

The 8-day old 3D-organoid cultures were fixed with 4% formaldehyde and permeabilized using 0.5% cold Triton X-100 solution. The fixed-organoid cultures were blocked using 10% BSA in PBS and subjected to indirect immunofluorescence staining using an E-cadherin antibody (Cell Signaling Technology, Canada) as the primary antibody and goat anti-rabbit antibody conjugated to Cy5 dye (Jackson Laboratories, Canada) as the secondary antibody. The organoids also were incubated with the filamentous (F) actin stain tetramethyl-rhodamine isothiocyanate (TRITC)-conjugated phalloidin (Millipore-Sigma, Canada) and the DNA fluorescent dye Hoechst 33342 (Invitrogen, Canada) to visualize the actin cytoskeleton and nuclei, respectively, of cells. The slides were mounted, and fluorescence images of the multicellular colonies were captured using a fluorescence microscope with a 40× objective lens (Olympus Fluoview FV1000 microscope, Canada). Exposure times for E-cadherin, F-actin, and Hoechst-specific signals were kept constant in each experiment [24, 25, 32, 34]. Images of 2 to 3 organoids per experimental condition were captured out of more than six qualitatively-assessed organoids. TRITC-phalloidin stained multicellular structures were quantified for cortical actin organization and presented graphically.

Migration-Scratch assay

A scratch assay was used to assess the migratory abilities of the MDA-MB-231 breast cancer cells under different conditions. To achieve this 0.5 ml 10% FBS-growth medium containing 5×10^5 cells was added per well of a 12-well tissue culture plate that was kept in a 5% CO₂ humidified incubator at 37°C incubator for 24 h to allow cell monolayers reach near confluency. Confluent MDA-MB-231 cell monolayers were then washed and incubated at 37°C in 0.2% FBS-containing DMEM medium overnight (serum starvation). Cells were removed along the midline of the serum-starved cell monolayers in each well using a 200 µL pipette tip (scratch), followed by a PBS wash to remove floating cells, and incubating the remaining monolayers under serum starvation, without or with 100 pM final concentration of TGFβ, for 30 h in a 5% CO₂ humidified incubator at 37°C. Cells and enclosing scratch were imaged at 4× objective of a DIC microscope (Olympus IX70) coupled to a digital camera at time 0 h and 30 h after initiating the scratch. To assess scratch width and closure, three images were obtained along the vertical axis of each scratch per well, and the width of the scratch (empty space) at three distinct positions per image were measured using ImageJ (National Institutes of Health, USA), averaged for the nine measurements per well. Scratch closure per well, i.e., experimental condition, is determined by subtracting the average width at 30 h from that at 0 h and expressing the difference relative to average width at 0 h.

Statistical analyses

Replicates are used to account for intra-experimental variations in measurements of a particular parameter, which may otherwise lead to erroneous hypothesis testing and parameter estimation. Biological replicates incorporate the use of biologically distinct samples or cell culture populations in a specific type of experiment and are used to alleviate random biological variations which may be a source of noise or be part of the subject of study [35]. A minimum of three biological replicates were used for each type of experiment in studies described in this manuscript, except where stated, to facilitate statistical inference. Unpaired Student's t-test (for two groups) or One-way analysis of variance (ANOVA) followed by Tukey-Kramer post-test (for more than two groups) using InStat (GraphPad InStat, San Diego, CA, USA) were performed to evaluate the statistical significance of data from biological replicates per experiment where appropriate. Values of $P \leq 0.05$ were considered statistically significant. Data are presented graphically as mean \pm standard error of the mean (SEM) for experiments with a minimum of three biological replicates.

RESULTS

Sumoylated SnoN suppresses TGFβ-induced EMT in mammary epithelial organoids

The activated TGFβ-receptor complex induces the C-terminal phosphorylation of Smad2 and Smad3, which in turn transduce the signal from the cytoplasm to the nucleus leading to regulation of gene expression programs including those that promote EMT [9–11]. SnoN regulates TGFβ signaling by interacting with Smad2/3 raising the question of whether sumoylation of SnoN regulates the ability of Smad proteins to promote EMT. We first determined

the role of SnoN in Smad-mediated EMT in non-transformed NMuMG mammary epithelial cells, because these cells represent a good model for studies of EMT [14, 24, 25, 32]. NMuMG cells cultured in the context of extracellular matrix (ECM) lead to organoids with a hollow lumen or acini. EMT-related changes manifest as morphological changes including lumen filling and/or deformation, loss or mislocalization of the epithelial marker E-cadherin, and loss or reduction in the cortical actin phenotype to a more diffused actin cytoskeleton (Fig. 1B–D, S1A–C) [24, 25, 33]. The protein SnoNKdR is a sumoylation-defective SnoN as the SUMO acceptor Lysine residues 50 and 383 are converted to arginine, which lacks the ability to be conjugated by SUMO [14, 24–26]. As expected, expression of SnoNKdR (Fig. 1A) promoted EMT-related changes including filling, deformation, E-cadherin loss/mislocalization, and cortical actin loss/reduction in the NMuMG organoid acini even in the absence of exogenous TGFβ (Fig. 1B–D, S1A–C) [24, 25]. In addition, small hairpin (sh) RNA-knockdown of endogenous Smad2 (Smad2i), Smad3 (Smad3i), alone or together (Fig. 1A) suppressed these TGFβ-EMT-like effects in three-dimensional NMuMG cell-derived organoids [32]. Importantly, knockdown of endogenous Smad2/3 led to significant suppression of SnoNKdR-induced EMT-related responses in NMuMG organoids (Fig. 1A–D, S1A–C).

The SUMO-SnoN fusion acts as SUMO gain of function SnoN including in EMT [24–26]. Accordingly, SUMO-SnoN (Fig. 2A) suppressed exogenous TGFβ-induced filling and/or disorganization, loss/mislocalization of E-cadherin, and loss/reduction of cortical actin organization in the 3D-NMuMG cell-derived organoids (Fig. 2B–D, S2A–C) [25]. Importantly, expression of SUMO-SnoN suppressed the ability of overexpressed Smad2 and Smad3 (Fig. 2A) to induce EMT-like responses in the non-transformed mammary epithelial cell-derived organoids (Fig. 2B–D, S2A–C). Collectively, these data suggest that SnoN suppresses TGFβ-induced EMT-related effects in mammary epithelial cells in a Smad-dependent manner.

We asked whether sumoylation affects the ability of SnoN to interact with Smad proteins. SnoN interacts with Smad2/3 and Smad4 via distinct regions in SnoN [36, 37]. SnoN interacted with Smad2 and Smad4 in the presence of constitutively activated TGFβ receptor I (TβRI TD) (Fig. 2E, S2D) [15, 38, 39]. However, both SnoNKdR and wild type SnoN associated effectively with Smad2 and Smad4. These data suggest that sumoylation has little or no effect on the association of SnoN with Smad proteins.

Sumoylation regulates the ability of SnoN to associate with histone acetylation modulators with functional significance for EMT induction in epithelial cell-derived organoids

SnoN interacts with HDAC1 and thereby inhibits Smad-dependent transcription [15, 21]. We asked whether sumoylation affects the association of SnoN with HDAC1. To address this question, we assessed the ability of the SUMO loss of function SnoNKdR and SUMO gain of function SUMO-SnoN, to associate with HDAC1 using Renilla luciferase-based coimmunoprecipitation assays. We confirmed that SnoN interacts with HDAC1 (Fig. 3A, S3A). We found that SnoNKdR interacted less effectively, and SUMO-SnoN interacted more effectively, as compared to wild type SnoN, with HDAC1 (Fig. 3A). Thus, these data suggest that sumoylation promotes the association of SnoN with HDAC1.

We next asked the functional consequences of the effect of sumoylation on SnoN-HDAC1 interaction. We first characterized the role of HDAC1 in the morphogenesis of mammary epithelial cell-derived organoids and in relationship to TGFβ-induced EMT. Increasing the protein abundance of HDAC1, even modestly (Fig. 3B), in cells suppressed exogenous TGFβ-induced EMT, as indicated by presence of hollow center, decreased deformation, maintenance of protein abundance and junctional localization of E-cadherin, and of cortical actin phenotypes of the NMuMG cell-derived acini (Fig. 3C–E, S3B–D). Conversely, RNAi-induced

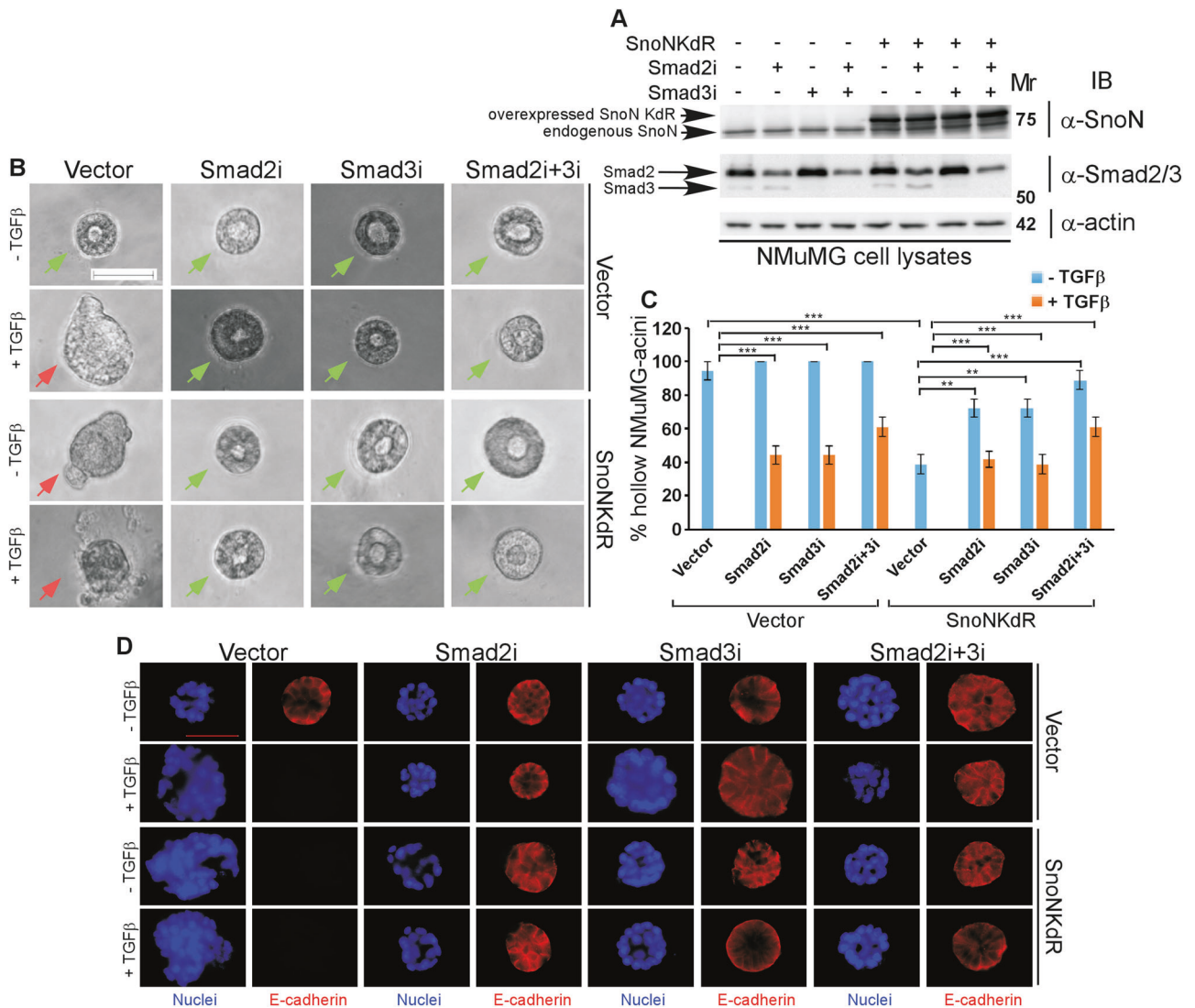


Fig. 1 TGF β -Smad2/3 pathway mediates the ability of the non-sumoylated SnoN to induce EMT in mammary epithelial organoids. **A** Smad2/3, SnoN, and actin (loading control) immunoblotting (IB) of lysates of NMuMG cells transfected with a stable vector control (–) or a plasmid stably expressing the SUMO loss of function SnoNKdR (+), with each transiently transfected with a control RNAi plasmid (–), or one expressing a Smad2-targeting shRNA Smad2i (+), a Smad3-targeting shRNA Smad3i (+), alone or together. **B** Representative differential contrast (DIC) light microscopy micrographs of live untreated (–) or 100 pM TGF β -treated (+) 8-day old organoids of NMuMG cells transfected and assessed as in **A**. Green and red arrows indicate hollow and filled acinar organoids, respectively. **C** Bar graph depicts mean \pm SEM proportion of hollow centred-acinar organoids expressed as a percentage of total colonies scored for each experimental condition from three biological replicates including the one with representative DIC images shown in **B**. **D** Representative fluorescence microscopy scans of E-cadherin (immunocytochemistry-red) and nuclei (Hoechst-blue) stained fixed 8-day old organoids of NMuMG cells transfected and assessed as in **A** to **C**. Mr indicates Markers' molecular size. Statistical difference, ANOVA: ** $P \leq 0.01$, *** $P \leq 0.001$. Scale bar indicates 50 μ m.

(HDAC1i) knockdown of endogenous HDAC1 (Fig. 3B) promoted an EMT-like phenotype in the 3D-NMuMG cell-derived acini, even in the absence of exogenous TGF β (Fig. 3C–E, S3B–D). Expression of the sumoylation-defective SnoNKdR reduced EMT suppression by overexpressed HDAC1, whereas knockdown of endogenous HDAC1 abrogated the ability of SnoN or SUMO-SnoN to suppress EMT-like behaviour of the three-dimensional mammary epithelial organoids (Fig. 3B–E, S3B–D). Together, these data suggest that endogenous HDAC1 suppresses TGF β -Smad-induced EMT-like effects in epithelial cell-derived organoids in a manner dependent on the sumoylation status of SnoN.

Next, we determined the role of HDAC1 deacetylase activity in mediating SnoN function in EMT. We first generated a deacetylase inactive HDAC1 mutant (HDAC1YH), in which the Tyrosine 303 residue was mutated to histidine [29]. SnoN associated more

robustly with the deacetylase-dead HDAC1YH as compared to the native HDAC1 (Fig. 4A, S4A). Importantly, the enzymatically inactive HDAC1YH (Fig. 4B) phenocopied HDAC1 knockdown in promoting EMT-associated changes in the NMuMG cell-derived organoids even in the absence of exogenous TGF β (Fig. 4C–E, S4B–D). Similarly, HDAC1YH decreased the ability of SnoN or SUMO-SnoN to suppress EMT induction by exogenous TGF β (Fig. 4C–E, S4B–D). These data suggest that HDAC1 acts in deacetylase-dependent manner to mediate SnoN suppression of exogenous TGF β -induced EMT-associated phenotypes in mammary epithelial cell-derived organoids (Fig. 4B–E, S4B–D). In other analyses, we found that induction of EMT upon knockdown of endogenous HDAC1 or increased expression of the deacetylase-inactive HDAC1YH (Fig. S5A–B) was reversed by incubation of the NMuMG organoid cultures with a TGF β type I receptor kinase

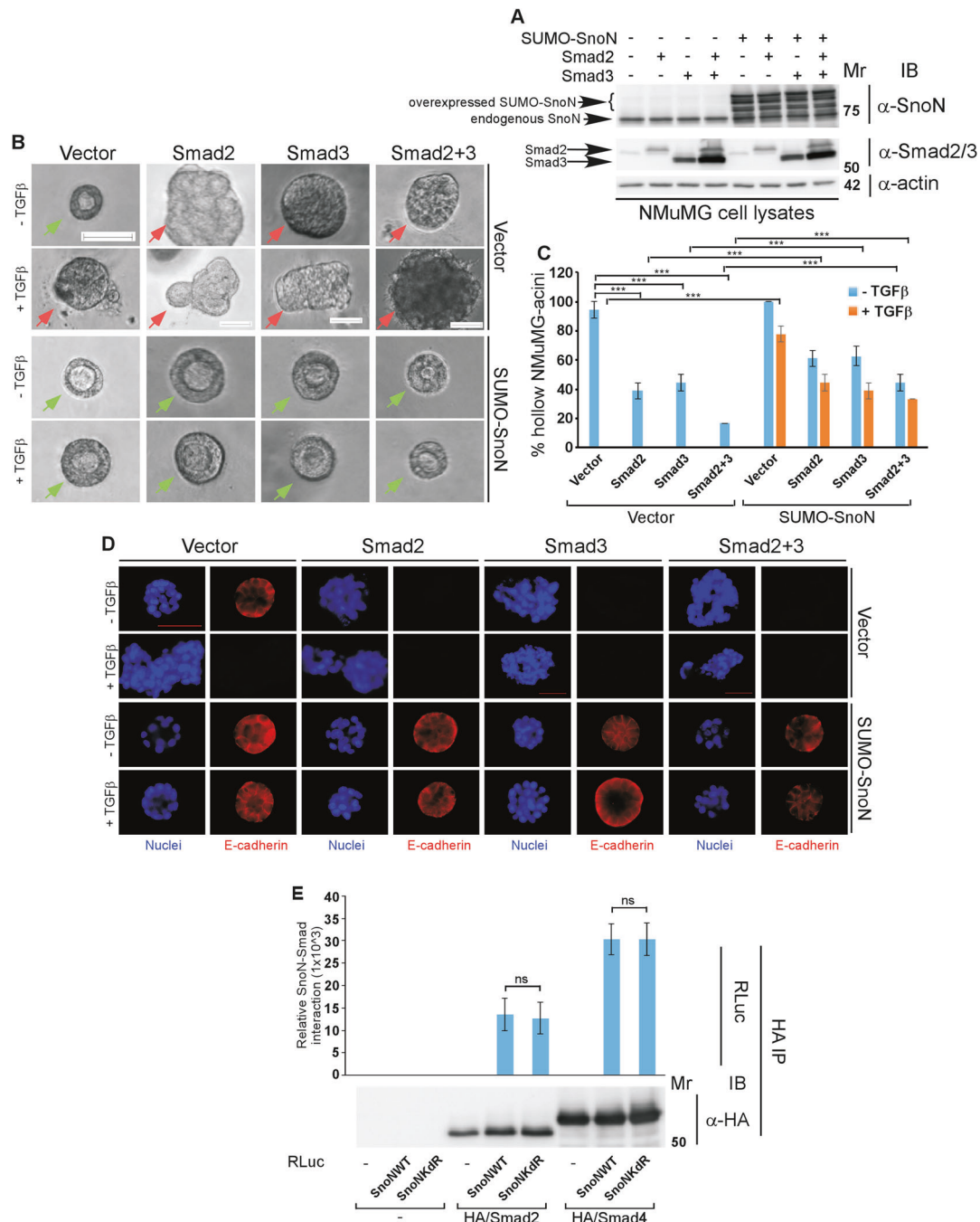


Fig. 2 Sumoylation is important for SnoN to suppress Smad2/3-induced EMT but not SnoN-Smad association. **A–D** SUMO gain of function SnoN antagonizes EMT induction by expressed Smad2/3. **A** Smad2/3, SnoN, and actin (loading control) immunoblotting (IB) of lysates of NMuMG cells transfected with a stable vector control (–), or a plasmid stably expressing the SUMO gain of function SnoN SUMO-SnoN (+), with each transiently transfected with a vector control (–), or a plasmid expressing Smad2 (+) or Smad3 (+), alone or together. **B** Representative differential interference contrast (DIC) light microscopy micrographs of live untreated (–) or 100 pM TGFB-treated (+) 8-day old organoids of NMuMG cells transfected and assessed as in **A**. Green and red arrows indicate hollow or filled acinar organoids, respectively. **C** Bar graph depicts mean \pm SEM proportion of hollow acinar organoids expressed as a percentage of total colonies counted for each experimental condition from three biological replicates including the replicate with representative DIC images shown in **B**. **D** Representative fluorescence microscopy scans of E-cadherin (immunocytochemistry-red) and nuclei (Hoechst-blue) stained fixed 8-day old organoids of NMuMG cells transfected and assessed as in **A** to **C**. **E** Sumoylation does not impact SnoN-Smad interaction. Lysates of HEK293T cells transfected with a plasmid encoding only the protein Renilla luciferase (RLuc) (–), or in fusion with the wild type SnoN (SnoNWT), or the SUMO loss of function SnoNkdR, together with a vector control (–) alone, or a plasmid encoding an hemagglutinin-tagged Smad2 (HA/Smad2) or Smad4 (HA/Smad4), and a plasmid encoding a constitutively active TGFB type I receptor kinase in which Threonine 204 is converted to aspartate (T β RI TD), were subjected to Smad2/Smad4 immunoprecipitation (α -HA IP), followed by Renilla luciferase assay (RLuc) or Smad immunoblotting (α -HA IB) of 80% and 20%, respectively, of the Smad immunocomplexes. Graphical data show mean \pm SEM (three biological replicates) of luciferase activity coimmunoprecipitated by Smad2/4 expressed relative to its respective input luciferase activity. Mr indicates Markers' molecular size. Statistical difference, ANOVA: *** $P \leq 0.001$, ns not significant. Scale bar indicates 50 μ m.

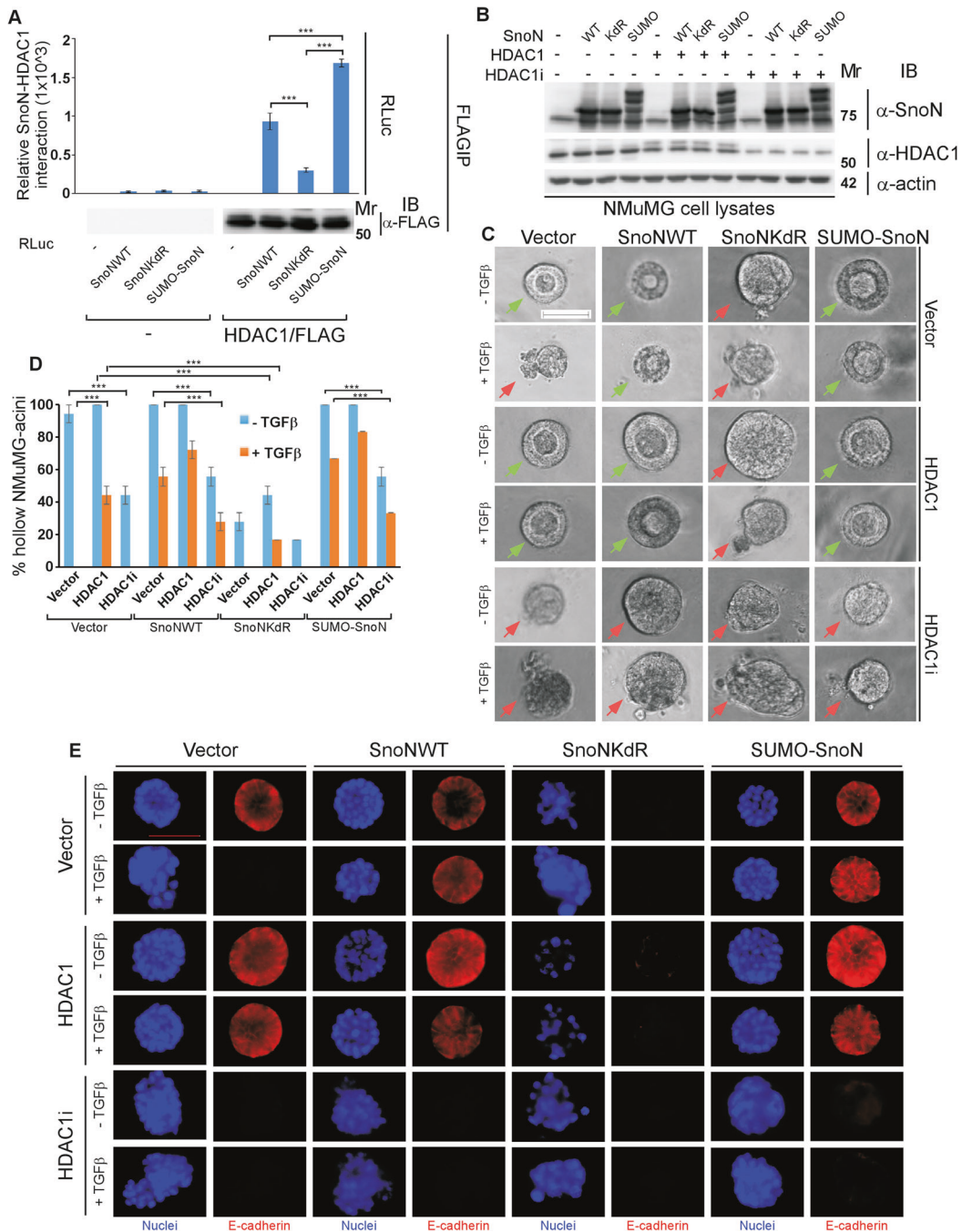
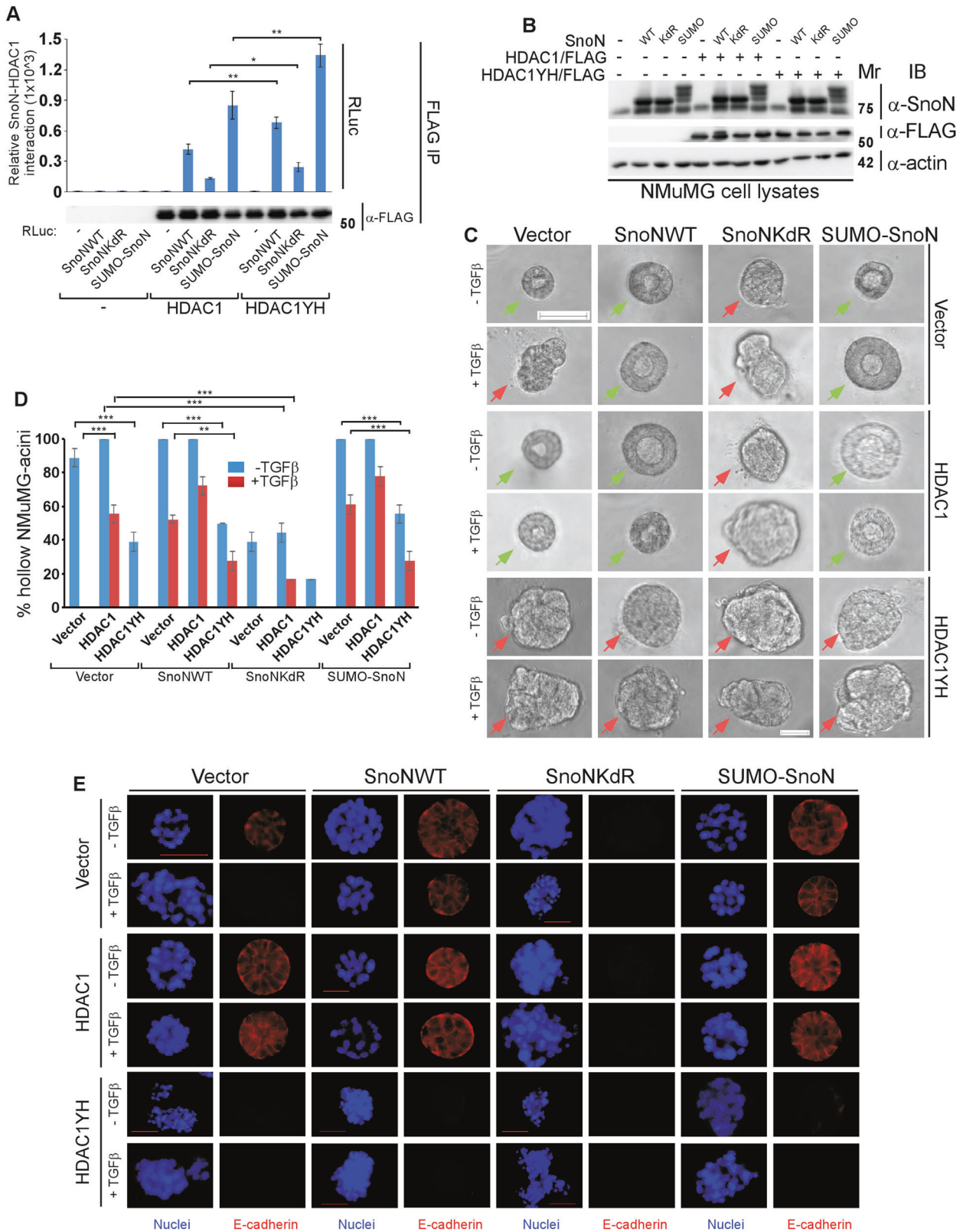


Fig. 3 Sumoylation promotes SnoN interaction with HDAC1, to suppress TGFβ-induced EMT. **A** Sumoylation enhances SnoN-HDAC1 association. Lysates of HEK293T cells transfected with a plasmid encoding only the protein Renilla luciferase (RLuc) (-), or in fusion with the wild type SnoN, the SUMO loss of function SnoNKdR, or the SUMO gain of function SUMO-SnoN, together with a control vector (-), or a plasmid encoding a C-terminally FLAG-tagged HDAC1 (HDAC1/FLAG), were subjected to HDAC1 immunoprecipitation (α-FLAG IP), followed by Renilla luciferase assay (RLuc) or HDAC1 immunoblotting (α-FLAG IB) of 80% and 20%, respectively, of the HDAC1 immunocomplexes. Graphical data show mean ± SEM (three biological replicates) of luciferase activity coimmunoprecipitated by HDAC1 expressed relative to its respective input luciferase activity. **B–E** Sumoylated SnoN acts via HDAC1 to suppress EMT in mammary epithelial organoids. **B** SnoN, HDAC1 and actin (loading control) immunoblotting (IB) of lysates of NMuMG cells transfected with a stable vector control (-), or a plasmid stably expressing the wild type SnoN (WT), the SUMO loss of function SnoNKdR (KdR), or the SUMO gain of function SUMO-SnoN (SUMO), with each transiently transfected with vector controls (-), or a plasmid expressing the protein HDAC1 (+), or one encoding the HDAC1-targetting shRNA HDAC1i (+). **C** Representative differential interference contrast (DIC) light microscopy micrographs of live untreated (-) or 100 pM TGFβ-treated (+) 8-day old organoids of NMuMG cells transfected and assessed as in **B**. Green and red arrows indicate hollow and filled/disorganized acinar organoids, respectively. **D** Bar graph depicts mean ± SEM of proportion of hollow acinar organoids expressed as a percentage of total colonies scored for each experimental condition from three biological replicates including the replicate with representative DIC images shown in **C**. **E** Representative fluorescence microscopy scans of E-cadherin-(immunocytochemistry-red) and nuclei-(Hoechst-blue) stained of fixed 8-day old organoids of NMuMG cells transfected and assessed as in **B–D**. Mr indicates Markers' molecular weight. Statistical difference, ANOVA: ***P ≤ 0.001. Scale bar indicates 50 μm.



(T β RI) inhibitor (KI) (Fig. S5C–E). These data suggest that endogenous HDAC1 acts in a deacetylase-dependent manner to suppress the ability of endogenous/basal TGF β -Smad signaling to induce EMT-related plastic effects in epithelial cell-derived

organoids (Fig. S5C–E). Collectively, these findings suggest that sumoylation enhances the SnoN-HDAC1 association, which in turn suppresses, in an HDAC1 deacetylase-dependent manner, TGF β -induced EMT in epithelial cell-derived organoids.

Fig. 4 Sumoylated SnoN suppresses, in an HDAC1 deacetylase activity-dependent manner, TGF β -induced EMT of mammary epithelial organoids. **A** Effect of HDAC1 acetylase activity on association with SnoN. Lysates of HEK293T cells transfected with a plasmid encoding only the protein Renilla luciferase (RLuc) (–), or in fusion with the wild type SnoN, the SUMO loss of function SnoNKdR, or the SUMO gain of function SUMO-SnoN, together with a control vector (–), or a plasmid encoding HDAC1/FLAG or the deacetylase inactive HDAC1YH/FLAG, were subjected to HDAC1 immunoprecipitation (α -FLAG IP), followed by Renilla luciferase assay (RLuc) or HDAC1 immunoblotting (α -FLAG IB) of 80% and 20%, respectively, of the HDAC1 immunocomplexes. Graphical data show mean \pm SEM (three biological replicates) of luciferase activity coimmunoprecipitated by HDAC1 expressed relative to its respective input luciferase activity. **B–E** *DAC1* acts in a deacetylase-dependent manner to mediate sumoylated SnoN-HDAC1 suppression of EMT. **B** SnoN, HDAC1 and actin (loading control) immunoblotting (IB) of lysates of NMuMG cells transfected with a stable vector control (–), or a plasmid stably expressing the wild type SnoN (WT), the SUMO loss of function SnoNKdR (KdR), or the SUMO gain of function SUMO-SnoN (SUMO), with each transfected transiently with a vector control (–), or a plasmid encoding HDAC1 (+) or the deacetylase inactive HDAC1YH (+). **C** Representative differential interference contrast (DIC) light microscopy micrographs of untreated (–) or 100 pM TGF β -treated (+) 8-day old organoids of NMuMG cells transfected and assessed as in **B**. Green and red arrows indicate acinar and filled organoids, respectively. **D** Bar graph depicts mean \pm SEM proportion of acinar organoids expressed as a percentage of total colonies counted for each experimental condition from three biological replicates including the replicate with the representative DIC images shown in **C**. **E** Representative fluorescence microscopy scans of E-cadherin-(immunocytochemistry-red) and nuclei-(Hoechst-blue) stained of fixed 8-day old organoids of NMuMG cells transfected and assessed as in **B–D**. Mr indicates Markers' molecular size. Statistical difference, ANOVA: * $P \leq 0.05$, ** $P \leq 0.01$, *** $P \leq 0.001$. Scale bar indicates 50 μ m.

Sumoylated SnoN suppression of TGF β -induced EMT involves regulation of function of acetyl transferase p300

The histone acetyltransferase p300 that promotes histone acetylation and regulates chromatin compactness, interacts with SnoN and thereby regulates gene expression regulation [16, 40]. We, therefore, determined if sumoylation of SnoN modulates the SnoN-p300 association. Luciferase-based coimmunoprecipitation analysis confirmed that SnoN and the SUMO gain of function SUMO-SnoN associate similarly with p300, whereas the SUMO loss of function SnoNKdR showed approximately 40% reduction in its ability to interact with p300 (Fig. 5A and S6A). These data suggest that sumoylation promotes SnoN-p300 complex formation (Fig. 5A).

That sumoylation enhances SnoN association with p300 raised the question of functional implication of this modification-enhanced interaction. To address this question, we focused on TGF β -induced EMT. We found that p300 expression promoted, whereas knockdown of p300 (Fig. 5B) suppressed exogenous TGF β -induced EMT-like phenotype in three-dimensional NMuMG epithelial-derived organoids indicating that p300 is required for EMT induction by TGF β (Fig. 5C–E, S6B–D). Importantly, whereas expression of SnoN or SUMO-SnoN suppressed p300-induced EMT-like changes, SnoNKdR failed to promote EMT in p300-knockdown cell-derived organoids (Fig. 5B–E, S6B–D). In other experiments, the promotion of EMT upon expression of p300 required active endogenous/basal TGF β signaling (Fig. S6E–H). Altogether, these data suggest that SnoN acts in a sumoylation-dependent manner to associate with p300 and thereby inhibits the ability of p300 to promote TGF β -induced EMT-like behaviour in epithelial cell-derived organoids.

Sumoylated SnoN regulates histone acetylation modulators to suppress TGF β -induced EMT-related phenotypes in breast carcinoma organoids

That SnoN associates in a sumoylation-dependent manner with HDAC1 and p300 raised the question of the functional consequences of this interaction in cancer cells (Figs. 3–5). EMT plays key roles in the invasion and metastasis of carcinomas including in breast cancer. SnoN acts in a sumoylation-dependent manner to suppress TGF β -induced EMT-associated responses including invasive growth of human breast cancer cells [25, 26]. We asked whether sumoylated SnoN suppression of EMT in cancer cells is mediated by regulation of HDAC1 and/or p300 in the human triple negative breast cancer MDA-MB-231 cells. Activation of TGF β signaling induces the ubiquitination and consequent degradation of SnoN in cells [38]. We first characterized if the ability of TGF β signaling to reduce SnoN protein levels is sumoylation-dependent (Fig. 6A, B). Immunoblotting analyses in MDA-MB-231 cells suggested that SnoN's sumoylation status has little or no effect

on TGF β signaling-mediated reduction in SnoN protein abundance (Fig. 6A, B). We next characterized the interplay between sumoylated SnoN and Smad2/3 in EMT in the MDA-MB-231 organoids. When cultured in the context of an extracellular matrix source, MDA-MB-231 cells organize into organoids showing a spherical phenotype with filled centre, reflecting the transformed nature of these cells [25, 26, 31, 33, 34]. TGF β -induced EMT-associated morphogenetic changes manifested as deformation, budding and invasive growth (Figs. 6–8, S7, S8, S10), and loss of protein abundance of the epithelial marker E-cadherin, and cortical actin of MDA-MB-231 organoids (Fig. 7D, S8A, B, and [25, 34]) As expected, we found that expression of the SUMO loss of function SnoNKdR (Fig. 6C) promoted an EMT-associated response even in the absence of exogenous TGF β in three-dimensional MDA-MB-231 cell-derived organoids (Fig. 6D, E). Knockdown of endogenous Smad2, Smad3, alone or together (Fig. 6C) suppressed TGF β -induced EMT-like effects in MDA-MB-231 organoids (Fig. 6D, E). Importantly, knockdown of endogenous Smad2/3 reduced the ability of SnoNKdR to promote EMT in MDA-MB-231 organoids in the absence or presence of exogenous TGF β (Fig. 6D, E). Conversely, expression of Smad2, Smad3, alone or together (Fig. 6F) promoted an EMT-like phenotype even in the absence of exogenous TGF β in breast carcinoma organoids (Fig. 6G–H). Expression the SUMO gain of function SUMO-SnoN (Fig. 6F), as expected, suppressed the ability of exogenous TGF β to induce EMT in breast carcinoma organoids (Fig. 6G–H) [25]. Importantly, SUMO-SnoN suppressed the ability of overexpressed Smad2 and Smad3 to promote EMT in breast carcinoma organoids (Fig. 6G–H). Together, these data suggest that SnoN acts in a Smad-dependent manner to regulate TGF β -induced EMT responses in MDA-MB-231 breast carcinoma organoids (Fig. 6C–H).

Next, we investigated the role of HDAC1 on TGF β -induced EMT in three-dimensional MDA-MB-231 breast carcinoma-derived organoids. Expression of HDAC1 (Fig. S7A), even modestly, decreased the EMT-associated invasive growth phenotype of MDA-MB-231 organoids in the absence or presence of exogenous TGF β (Fig. S7B, C). Conversely, knockdown of endogenous HDAC1 (Fig. S7A) promoted an EMT-like phenotype in breast carcinoma organoids even in the absence of exogenous TGF β (Fig. S7B, C). Expression of the sumoylation-defective SnoNKdR (Fig. S7A) reduced the ability of HDAC1 to suppress TGF β -induced EMT-associated invasive growth of the breast carcinoma-derived organoids (Fig. S7B, C). On the other hand, endogenous HDAC1 knockdown (Fig. S7A) reduced the ability of SUMO-SnoN to suppress TGF β -induced EMT-like phenotype of the breast carcinoma organoids (Fig. S7B, C). Together, these data suggest that sumoylated SnoN acts in an HDAC1-dependent manner to suppress TGF β -Smad-induced EMT in breast carcinoma organoids.

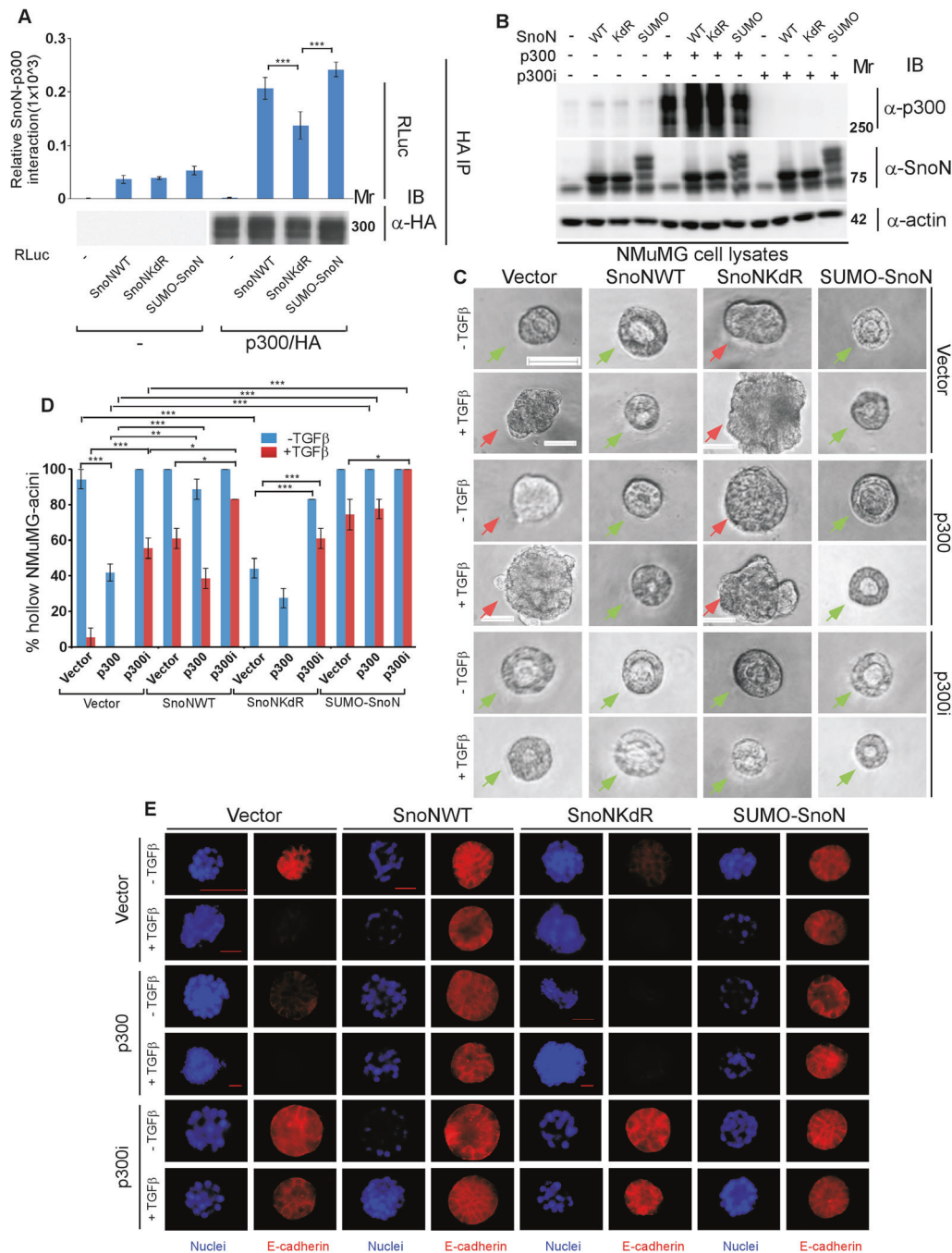
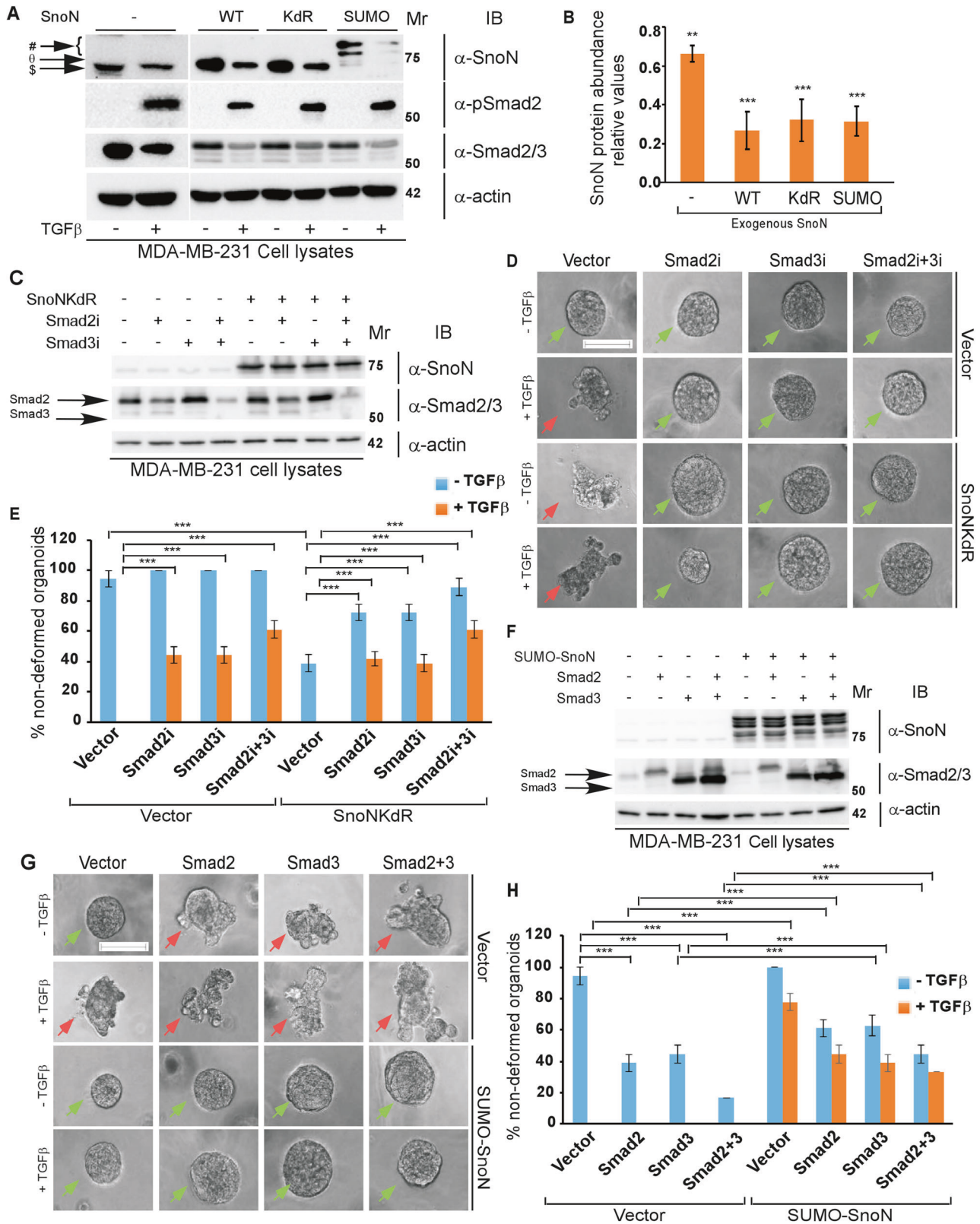


Fig. 5 Sumoylation promotes SnoN-p300 interaction to suppress TGFβ-induced EMT in mammary epithelial organoids. **A** Sumoylation promotes SnoN-p300 association. Lysates of HEK293T cells transfected with a plasmid encoding only the protein Renilla luciferase (RLuc) (–), or in fusion with the wild type SnoN, the SUMO loss of function SnoNKdR, or the SUMO gain of function SUMO-SnoN, together with a control vector (–), or a plasmid expressing a C-terminally HA-tagged p300 (p300/HA), were subjected to p300 immunoprecipitation (α-HA IP), followed by Renilla luciferase assay (RLuc) or p300 immunoblotting (α-HA IB) of 80% and 20%, respectively, of the p300 immunocomplexes. Graphical data show mean ± SEM (three biological replicates) of luciferase activity coimmunoprecipitated by p300, expressed relative to its respective input luciferase activity. **B–E** Sumoylated SnoN suppresses p300-induced EMT in mammary epithelial organoids. **B** SnoN, p300 and actin (loading control) immunoblotting (IB) of lysates of NMuMG cells transfected with a stable vector control (–), or a plasmid stably expressing the wild type SnoN (WT), the SUMO loss of function SnoNKdR (KdR), or the SUMO gain of function SUMO-SnoN (SUMO), with each transfected transiently with vector controls (–), or a plasmid encoding the protein p300/HA (+), or the p300-targetting shRNA p300i (+). **C** Representative differential interference contrast (DIC) light microscopy micrographs of untreated (–) or 100 pM TGFβ-treated (+) 8-day old organoids of NMuMG cells transfected and assessed as in **B**. Green and red arrows indicate acinar and filled organoids, respectively. **D** Bar graph depicts mean ± SEM proportion of acinar organoids expressed as a percentage of total colonies counted for each experimental condition from three biological replicates including the replicate with representative DIC images shown in **C**. **E** Representative fluorescence microscopy scans of E-cadherin (immunocytochemistry-red) and nuclei (Hoechst-blue) stained of fixed 8-day old organoids of NMuMG cells transfected and assessed as in **B–D**. Mr indicates Markers' molecular size. Statistical difference, ANOVA: * $P \leq 0.05$, *** $P \leq 0.001$. Scale bar indicates 50 μm.



We next determined the role of the histone deacetylase activity of HDAC1 in suppression of EMT-associated effects in breast carcinoma organoid. Expression of the enzymatically inactive HDAC1YH (Fig. 7A) phenocopied HDAC1 knockdown in promoting EMT, as indicated by the invasive growth and loss of the protein

abundance of the epithelial marker E-cadherin, and loss of the cortical actin organization phenotypes in three-dimensional MDA-MB-231 cell-derived organoids, even in the absence of exogenous TGF β (Fig. 7B–D, S8A, B). Importantly, HDAC1YH decreased SUMO-SnoN suppression of EMT in breast carcinoma organoids

Fig. 6 TGF β -Smad2/3 pathway is a key target of SnoN suppression of EMT-associated responses in breast carcinoma organoids. **A, B** Impact of SnoN sumoylation status on reduction of SnoN protein level by TGF β signaling. **A** SnoN, TGF β -phosphorylated Smad2 on Serine residues 465 and 467 (pSmad2), Smad2/3, and actin (loading control) immunoblotting (IB) of lysates of MDA-MB-231 cells transfected with a stable vector control (–) or a plasmid stably expressing wild type SnoN (WT), SUMO loss of function SnoNKdR (KdR), or SUMO gain of function SUMO-SnoN (SUMO), incubated without (–) or with 100pM TGF β (+) for 6 h. SnoN-immunoreactive protein species are indicated in the upper blot corresponding to endogenous SnoN (\$ – 120 s exposure), exogenous SnoN (WT or KdR) (⊖) and SUMO-SnoN (#) (5 s exposure), MDA-MB-231 cell extracts with (+) and without (–) exogenous TGF β . **B** Bar graph depicts mean \pm SEM of actin-normalized SnoN immunoreactive species intensity in lysates from one of the four TGF β -treated MDA-MB-231 stables expressed relative to the untreated corresponding pair, obtained from three independent experiments including the one shown in 6A. Statistical difference, Unpaired Student's t-test: ** $P \leq 0.01$, *** $P \leq 0.00$, each compared to its corresponding untreated stable cells. **C–E** TGF β -Smad pathway mediates SnoNKdR-induction of EMT in breast carcinoma organoids. **C** SnoN, Smad2/3 and actin (loading control) immunoblotting (IB) of lysates of MDA-MB-231 cells transfected with a stable vector control (–) or plasmid stably expressing the SUMO loss of function SnoNKdR (+), with each transiently transfected with a control RNAi plasmid (–), or an RNAi plasmid expressing the Smad2-targeting shRNA Smad2i (+), the Smad3-targeting shRNA Smad3i (+), alone or together. **D** Representative differential interference contrast (DIC) light microscopy micrographs of untreated (–) or 100 pM TGF β -treated (+) 8-day old organoids of MDA-MB-231 cells transfected and assessed as in **C**. **E** Bar graph depicts mean \pm SEM proportion of non-deformed organoids expressed as a percentage of total colonies counted for each experimental condition from three biological replicates including the replicate with representative DIC images shown in **D**. **F, G** SUMO-SnoN antagonizes Smad2/3-induced EMT in breast carcinoma organoids. **F** SnoN, Smad2/3, and actin (loading control) immunoblotting (IB) of lysates of MDA-MB-231 cells transfected with a stable-vector control (–), or a plasmid stably expressing the SUMO gain of function SUMO-SnoN (+), with each transiently transfected with a vector control (–), or a plasmid encoding Smad2 (+) or Smad3 (+), alone or together. **G** Representative differential interference contrast (DIC) light microscopy micrographs of untreated or 100 pM TGF β -treated 8-day old organoids of MDA-MB-231 cells transfected and assessed as in **F**. **H** Bar graph depicts mean \pm SEM proportion of non-deformed organoids expressed as a percentage of total colonies counted for each experimental condition from three biological replicates including the replicate with the representative DIC images as shown in **G**. Green and red arrows indicate non-deformed and deformed organoids, respectively. Mr indicates Markers' molecular size. Statistical difference, ANOVA: *** $P \leq 0.001$. Scale bar indicates 50 μ m.

(Fig. 7A–D, S8A, B). These data suggest that the deacetylase activity of HDAC1 is required for SnoN to suppress TGF β -induced EMT behaviour in breast carcinoma organoids (Fig. 7A–D, S8A–B). In other analyses, promotion of EMT by RNAi-induced knockdown of HDAC1 and expression of the dominant negative deacetylase HDAC1YH required endogenous/basal TGF β -Smad signaling in the MDA-MB-231 organoids (Fig. S8C–F). Increased cell migration represents a feature of EMT. We therefore characterized the role of sumoylation in the effect of the SnoN-HDAC1 complex on MDA-MB-231 cell monolayers migration, in the absence and presence of exogenous TGF β using the scratch assay (Fig. S9A, B). As expected, exogenous TGF β promoted MDA-MB-231 cell migration (Fig. S9A, B). Expression of HDAC1 suppressed, whereas deacetylase-inactive HDAC1YH or knockdown of endogenous HDAC1 promoted TGF β -induced migration of MDA-MB-231 cells (Fig. S9A, B). We also found that expression of SnoNKdR promoted, whereas SUMO-SnoN suppressed TGF β -induced MDA-MB-231 cell migration (Fig. S9A, B). Importantly, SnoNKdR reversed HDAC1 suppression of migration, and conversely SUMO-SnoN reduced the ability of HDAC1YH or knockdown of endogenous HDAC1 to promote migration of these cells (Fig. S9A, B). These data further support the conclusion that the sumoylated SnoN-HDAC1 axis plays a key role in suppression of TGF β -induced EMT-associated effects (Fig. S9A, B). Collectively, these findings suggest that sumoylation enhances the SnoN-HDAC1 association, and in turn suppresses TGF β -induced EMT and associated responses in breast cancer cells.

We also determined the functional consequence of sumoylated SnoN-p300 interaction in the context of EMT in breast carcinoma organoids. Expression of p300 promoted, whereas knockdown of p300 suppressed, EMT morphogenetic changes in MDA-MB-231 organoids in the absence or presence of exogenous TGF β (Fig. 8A–C). Importantly, we found that overexpression of SUMO-SnoN suppressed the ability of p300 expression to induce EMT-like morphogenetic changes in the breast carcinoma organoids (Fig. 8A–C). Conversely, knockdown of p300 abrogated the ability of SnoNKdR to promote EMT in MDA-MB-231 carcinoma organoids (Fig. 8A–C). In other studies, the ability of expressed p300 to promote EMT-like effects in the MDA-MB-231 organoids required endogenous/basal TGF β -Smad signaling (Fig. S10A–C). We also characterized the functional consequences of the SnoN-p300 complex in regulating EMT using MDA-MB-231 cell migration

assays (Fig. S11A, B). We found that p300 expression promoted, whereas p300 knockdown suppressed the ability of TGF β to enhance migration of MDA-MB-231 cells (Fig. S11A, B). Interestingly, expression of SnoNKdR rescued the reduction in cell migration upon p300-knockdown (Fig. S11A, B). Conversely, SUMO-SnoN abrogated the ability of expressed p300 to promote MDA-MB-231 cell migration (Fig. S11A, B). Together, these data suggest that p300 promotes TGF β -induced EMT-associated morphogenetic phenotype and responses in breast cancer cells. In addition, SnoN sumoylation promotes SnoN-p300 association to suppress EMT in breast carcinomas.

Collectively, our study reveals that sumoylation promotes the ability of SnoN to associate with the histone acetylation modulators HDAC1 and p300 with functional implications for SnoN suppression of TGF β -Smad-induced EMT in mammary epithelial and carcinoma organoids. These findings add insights to the molecular mechanisms by which the SUMO pathway regulates biological processes in normal and disease states.

DISCUSSION

In this study, we have uncovered a novel link between the SUMO pathway and modulators of histone acetylation with important implications for regulation of EMT in epithelial and carcinoma organoids. We find that sumoylation of the transcription coregulator SnoN promotes its association with the histone deacetylase HDAC1 and the acetyl transferase p300. Endogenous HDAC1 suppresses, whereas endogenous p300 promotes EMT in epithelial and carcinoma organoids. Importantly, we find that SnoN acts in a sumoylation-dependent fashion to stimulate and inhibit, respectively, the effects of HDAC1 and p300 on EMT-associated morphological and functional changes in breast epithelial and carcinoma cells. Our findings should advance our understanding of the biology of the TGF β and sumoylation pathways.

The discovery that sumoylation promotes the ability of SnoN to associate with HDAC1 and p300 with opposing effects on their ability to regulate EMT provides mechanistic insights into how this modification enables SnoN to regulate EMT. These results help explain the critical role that sumoylation plays in SnoN suppression of Smad-mediated EMT. It will be interesting in future studies to characterize whether sumoylated SnoN regulates the

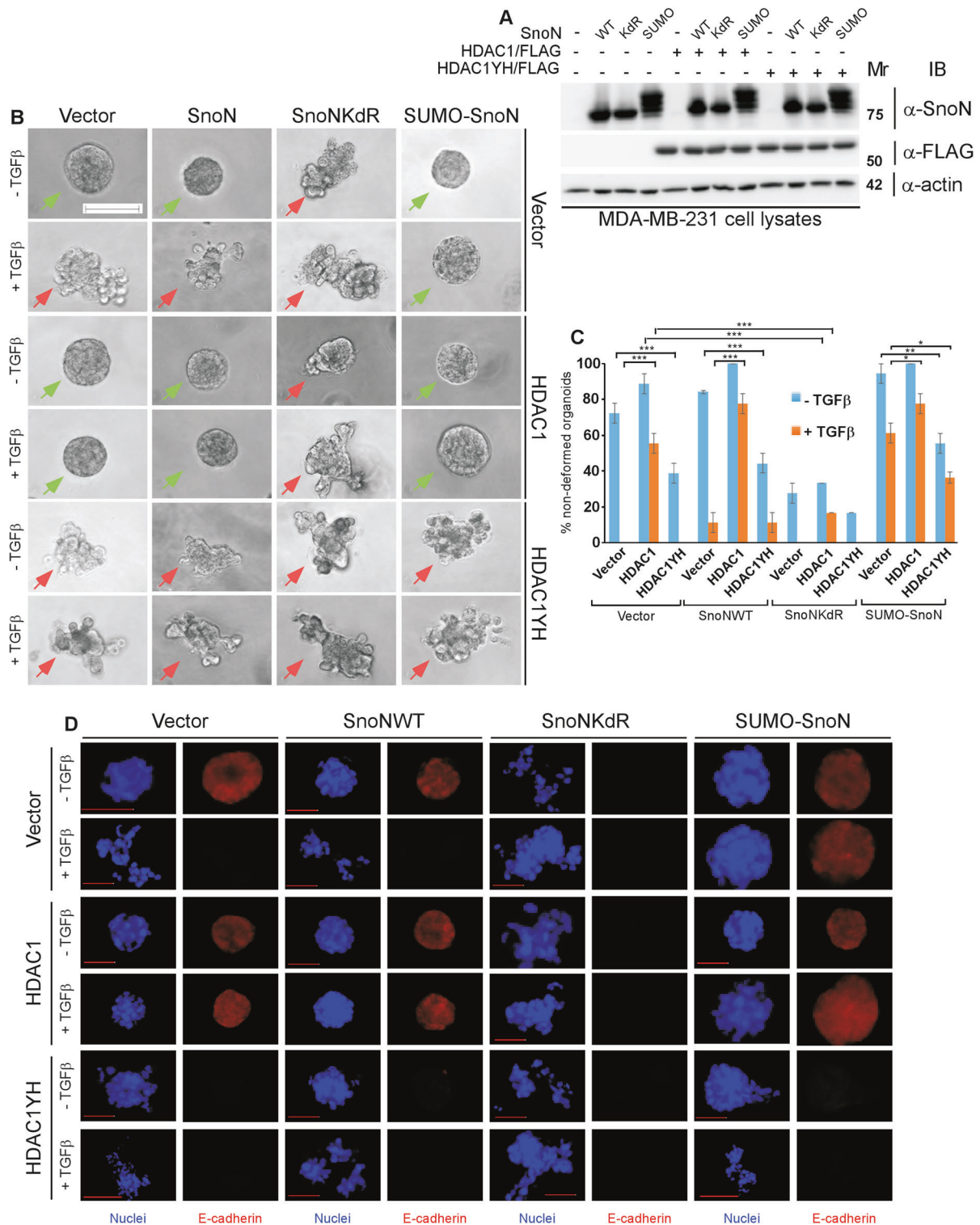


Fig. 7 HDAC1 acts in a deacetylase-dependent manner to mediate sumoylated SnoN suppression of EMT in breast carcinoma organoids. **A** SnoN, HDAC1 and actin (loading control) immunoblotting (IB) of lysates of MDA-MB-231 cells transfected with a stable vector control (–), or a plasmid stably expressing the wild type SnoN (WT), the SUMO loss of function SnoNKdR (KdR), or the SUMO gain of function SUMO-SnoN (SUMO), with each transiently transfected with a vector control (–), or a plasmid encoding HDAC1/FLAG (+) or the deacetylase inactive HDAC1YH/FLAG (+). **B** Representative differential interference contrast (DIC) light microscopy micrographs of untreated (–) or 100 pM TGFβ-treated (+) 8-day old organoids of MDA-MB-231 cells transfected and assessed as in **A**. Green and red arrows indicate non-deformed and deformed organoids, respectively. **C** Bar graph depicts mean ± SEM proportion of non-deformed organoids expressed as a percentage of total colonies counted for each experimental condition from three biological replicates including the replicate with the representative DIC images as shown in **B**. **D** Representative fluorescence microscopy scans of E-cadherin (immunocytochemistry-red) and nuclei (Hoechst-blue) stained of fixed 8-day old organoids of MDA-MB-231 cells transfected and assessed as in **A–C**. Mr indicates Markers' molecular size. Statistical difference, ANOVA: ** $P \leq 0.01$, *** $P \leq 0.001$. Scale bar indicates 50 μm.

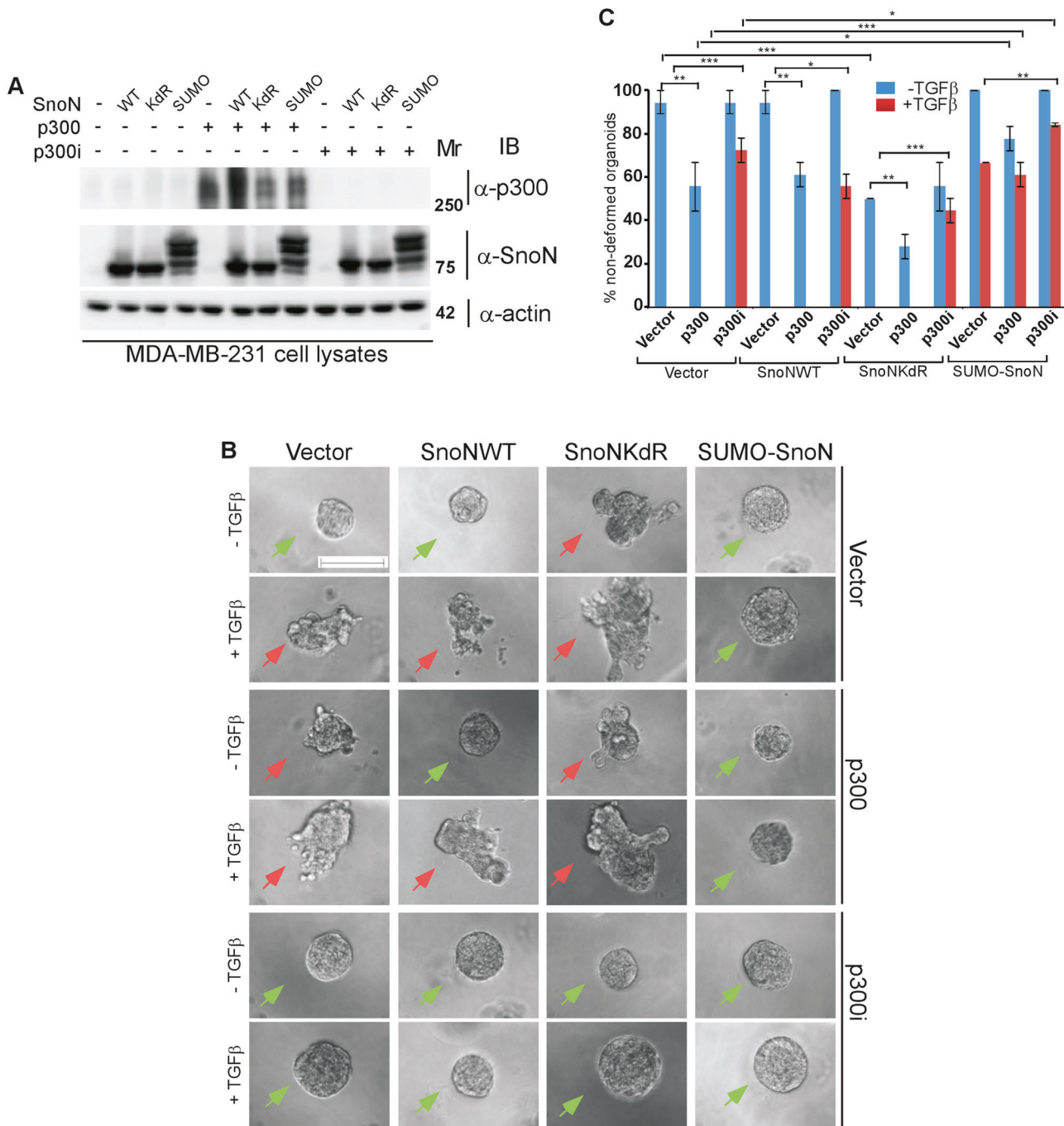


Fig. 8 Sumoylated SnoN suppresses p300-mediated EMT in breast carcinoma organoids. **A** p300, SnoN and actin (loading control) immunoblotting (IB) of lysates of MDA-MB-231 cells transfected with a stable vector control (-), or a plasmid stably expressing the wild type SnoN (WT), the SUMO loss of function SnoNKdR (KdR), or the SUMO gain of function SUMO-SnoN (SUMO), with each transfected transiently with vector controls (-), or a plasmid encoding the protein p300/HA (+), or the p300-targetting shRNA p300i (+). **B** Representative differential interference contrast (DIC) light microscopy micrographs of untreated (-) or 100 pM TGFβ-treated (+) 8-day old organoids of MDA-MB-231 cells transfected and assessed as in A. Green and red arrows indicate non-deformed and deformed organoids, respectively. **C** Bar graph depicts mean ± SEM proportion of non-deformed organoids expressed as a percentage of total colonies counted for each experimental condition from three biological replicates including the replicate with representative DIC images shown in **B**. Mr indicates Markers' molecular size. Statistical difference, ANOVA: * $P \leq 0.05$, ** $P \leq 0.01$, *** $P \leq 0.001$. Scale bar indicates 50 μm.

proportion of Smad-HDAC1- and Smad-p300-containing protein complexes in cells.

The finding that HDAC1 acts in a deacetylase-dependent manner to suppress TGFβ-Smad signaling-mediated EMT in the context of epithelial organoids contributes to better understanding of the biology of HDAC1. HDAC1 acts with distinct transcription factors to regulate the abundance of mRNA

encoding E-cadherin to promote or suppress EMT [41–43]. Interestingly, incubation of human adrenal cortical carcinoma cells with a class I HDAC inhibitor promotes EMT in these cells, supporting the idea that HDAC1 may act as a suppressor of EMT [44]. That HDAC1 suppresses EMT in a deacetylase-dependent manner, uncovered in the current study, is further supported by our finding that the histone acetylase p300 promotes EMT in

epithelial and carcinoma organoids, as well as increased TGF β -induced breast cancer cell migration, a key functional consequence of EMT. The protein p300 is thought to promote EMT in different tissue systems [16, 45–47]. p300 has been associated with cancer progression and poor prognosis in a number of tumor types [45–47], including breast cancer [48, 49]. Recently an inhibitor of p300-mediated Snail acetylation was reported to inhibit the growth and metastasis of p53-wild-type tumors [50]. It will be interesting to explore the extent of the antagonistic relationship between HDAC1 and p300 in controlling EMT in normal development and cancer pathogenesis.

The idea that sumoylated SnoN enables HDAC1 to act in a deacetylase-dependent manner to regulate TGF β -Smad-induced EMT has implications for the regulation of EMT. That the activity of HDAC1 is critical for sumoylated SnoN to suppress TGF β -induced EMT in non-transformed and transformed mammary epithelial organoids adds mechanistic insights into how posttranslational modification of SnoN can impact the ability of epigenetic regulators to modulate cellular processes. The SUMO loss of function SnoN, SnoNkdR has been shown to phenocopy endogenous SnoN knockdown in promoting EMT [14, 24, 32, 51]. Thus, that expression of SnoNkdR reduces the ability of HDAC1 to suppress TGF β -induced EMT suggests that HDAC1 suppression of EMT is regulated by the sumoylation status of endogenous SnoN. The lower HDAC1 binding capacity of non-sumoylated SnoN as compared to the sumoylated species may reduce HDAC1-containing Smad transcriptional regulatory complex with positive impact on EMT. TGF β -Smad signaling recruits distinct E3 ubiquitin-ligases including Smurf2, Arkadia and APC-Cdh1 to SnoN leading to its ubiquitination and consequent proteasomal degradation in different cell types [38, 52, 53]. It would be important to address if such mechanisms are involved in TGF β regulation of SnoN stability in the cellular models described here in future studies. Such future studies can be designed to characterize cell and context-based differences in the regulation of the protein abundance of SnoN by TGF β signaling, and specific molecular mechanisms involved and biological significance. Our finding that TGF β -reduction of SnoN protein level in breast cancer cells may not be affected by the sumoylation status of SnoN raises the key question whether TGF β signaling may act via other mechanisms to differentially regulate the abundance of sumoylated forms of SnoN in cells. Consistent with this idea, TGF β signaling has been shown to reduce the proportion of sumoylated species of SnoN to a greater extent than the unmodified form, by promoting the ubiquitin-mediated degradation of the SUMO E3 ligase PIAS1 in cells undergoing EMT [14, 26]. Overall, the potential differential reduction in sumoylated SnoN by TGF β signaling may disinhibit the effect HDAC1 on EMT in cells. Because SnoN recruits and forms a multiprotein complex with PIAS1 and TIF1 γ , the SUMO E3 ligase-complex may play a role in HDAC1's ability to suppress EMT.

The discovery that SnoN acts in a sumoylation-dependent manner to bind and differentially regulate HDAC1 and p300 opposing roles in EMT suggest that this modification provides a double-edged sword in suppressing this fundamental cellular process. It would thus be interesting to determine in future studies whether p300 and HDAC1 influence each other's association with SnoN. In addition, because HDAC1 and p300 form higher-order protein complexes including the epigenetic regulators Sin3A, NCoR, and the histone demethylases SETDB1, it will be interesting to investigate the possible physical and functional association of SnoN with these epigenetic factors in non-transformed and transformed cells derived from epithelial tissues in the context of EMT and other cellular responses.

The critical role of TGF β regulation of EMT plays in development and cancer highlights the importance of understanding the molecular mechanisms by which EMT is regulated. Our findings

add significant insights into how the SUMO pathway contributes to the regulation of EMT in epithelial cells.

DATA AVAILABILITY

All data are provided within the main text, figures, or supplementary materials. In addition, these analyses and original data are available from the corresponding author upon reasonable request.

REFERENCES

- Thiery JP, Cloque H, Huang RY, Nieto MA. Epithelial-mesenchymal transitions in development and disease. *Cell* 2009;139:871–90.
- Nieto MA, Huang RY, Jackson RA, Thiery JP. EMT: 2016. *Cell* 2016;166:21–45.
- Creighton CJ, Gibbons DL, Kurie JM. The role of epithelial-mesenchymal transition programming in invasion and metastasis: a clinical perspective. *Cancer Manag Res*. 2013;5:187–95.
- Kalluri R. EMT: when epithelial cells decide to become mesenchymal-like cells. *J Clin Invest*. 2009;119:1417–9.
- Ye X, Weinberg RA. Epithelial-mesenchymal plasticity: a central regulator of cancer progression. *Trends Cell Biol*. 2015;25:675–86.
- Moustakas A, Heldin CH. Mechanisms of TGF β -induced epithelial-mesenchymal transition. *J Clin Med*. 2016;5:63.
- Xu J, Lamouille S, Derynck R. TGF β -induced epithelial to mesenchymal transition. *Cell Res*. 2009;19:156–72.
- Shi Y, Massague J. Mechanisms of TGF β -signaling from cell membrane to the nucleus. *Cell* 2003;113:685–700.
- Itoh S, Itoh F, Goumans MJ, Ten, Dijke P. Signaling of transforming growth factor- β family members through Smad proteins. *Eur J Biochem*. 2000;267:6954–67.
- Derynck R, Akhurst RJ, Balmain A. TGF β -signaling in tumor suppression and cancer progression. *Nat Genet*. 2001;29:117–29.
- Massague J. TGF β in. *Cancer Cell* 2008;134:215–30.
- Bonni S, Bonni A. SnoN signaling in proliferating cells and postmitotic neurons. *FEBS Lett*. 2012;586:1977–83.
- Deheuninck J, Luo K. Ski and SnoN, potent negative regulators of TGF β -signaling. *Cell Res*. 2009;19:47–57.
- Netherton SJ, Bonni S. Suppression of TGF β -induced epithelial-mesenchymal transition like phenotype by a PIAS1 regulated sumoylation pathway in NMuMG epithelial cells. *PLoS one*. 2010;5:e13971.
- Stroschein SL, Wang W, Zhou S, Zhou Q, Luo K. Negative feedback regulation of TGF β -signaling by the SnoN oncoprotein. *Science* 1999;286:771–4.
- Ikeuchi Y, Stegmuller J, Netherton S, Huynh MA, Masu M, Frank D, et al. A SnoN-Ccd1 pathway promotes axonal morphogenesis in the mammalian brain. *J Neurosci*. 2009;29:4312–21.
- Sarker KP, Wilson SM, Bonni S. SnoN is a cell type-specific mediator of transforming growth factor- β responses. *J Biol Chem*. 2005;280:13037–46.
- Mizuide M, Hara T, Furuya T, Takeda M, Kusanagi K, Inada Y, et al. Two short segments of Smad3 are important for specific interaction of Smad3 with c-Ski and SnoN. *J Biol Chem*. 2003;278:531–6.
- Wallden K, Nyman T, Hallberg BM. SnoN stabilizes the SMAD3/SMAD4 protein complex. *Sci Rep*. 2017;7:46370.
- Wu JW, Krawitz AR, Chai J, Li W, Zhang F, Luo K, et al. Structural mechanism of Smad4 recognition by the nuclear oncoprotein Ski: insights on Ski-mediated repression of TGF β -signaling. *Cell* 2002;111:357–67.
- Nomura T, Khan MM, Kaul SC, Dong HD, Wadhwa R, Colmenares C, et al. Ski is a component of the histone deacetylase complex required for transcriptional repression by Mad and thyroid hormone receptor. *Genes Dev*. 1999;13:412–23.
- Johnson ES. Protein modification by SUMO. *Annu Rev Biochem*. 2004;73:355–82.
- Dohmen RJ. SUMO protein modification. *Biochim Biophys Acta*. 2004;1695:113–31.
- Ikeuchi Y, Dadakhujaev S, Chandhoke AS, Huynh MA, Oldenburg A, Ikeuchi M, et al. TIF1 γ protein regulates epithelial-mesenchymal transition by operating as a small ubiquitin-like modifier (SUMO) E3 ligase for the transcriptional regulator SnoN1. *J Biol Chem*. 2014;289:25067–78.
- Chanda A, Ikeuchi Y, Karve K, Sarkar A, Chandhoke AS, Deng L, et al. PIAS1 and TIF1 γ collaborate to promote SnoN SUMOylation and suppression of epithelial-mesenchymal transition. *Cell Death Differ*. 2021;28:267–82.
- Chanda A, Chan A, Deng L, Kornaga EN, Enwere EK, Morris DG, et al. Identification of the SUMO E3 ligase PIAS1 as a potential survival biomarker in breast cancer. *PLoS ONE*. 2017;12:e0177639.
- Taunton J, Hassig CA, Schreiber SL. A mammalian histone deacetylase related to the yeast transcriptional regulator Rpd3p. *Science*. 1996;272:408–11.

28. Pot I, Patel S, Deng L, Chandhoke AS, Zhang C, Bonni A, et al. Identification of a novel link between the protein kinase NDR1 and TGFbeta signaling in epithelial cells. *PLoS ONE*. 2013;8:e67178.
29. Lahm A, Paolini C, Pallaoro M, Nardi MC, Jones P, Neddermann P, et al. Unraveling the hidden catalytic activity of vertebrate class IIa histone deacetylases. *Proc Natl Acad Sci USA*. 2007;104:17335–40.
30. Kingston RE, Chen CA, Rose JK. Calcium phosphate transfection. *Curr Protoc Mol Biol*. 2003;Chapter 9:Unit 9 1.
31. Chandhoke AS, Chanda A, Karve K, Deng L, Bonni S. The PIAS3-Smurf2 sumoylation pathway suppresses breast cancer organoid invasiveness. *Oncotarget* 2017;8:21001–14.
32. Chandhoke AS, Karve K, Dadakhujaev S, Netherton S, Deng L, Bonni S. The ubiquitin ligase Smurf2 suppresses TGFbeta-induced epithelial-mesenchymal transition in a sumoylation-regulated manner. *Cell Death Differ*. 2016;23:876–88.
33. Dadakhujaev S, Salazar-Arcila C, Netherton SJ, Chandhoke AS, Singla AK, Jirik FR, et al. A novel role for the SUMO E3 ligase PIAS1 in cancer metastasis. *Oncoscience* 2014;1:229–40.
34. Sarkar A, Chanda A, Regmi SC, Karve K, Deng L, Jay GD, et al. Recombinant human PRG4 (rhPRG4) suppresses breast cancer cell invasion by inhibiting TGFbeta-Hyaluronan-CD44 signalling pathway. *PLoS ONE*. 2019;14:e0219697.
35. Blainey P, Krzywinski M, Altman N. Points of significance: replication. *Nat Methods*. 2014;11:879–80.
36. Tecalco-Cruz AC, Rios-Lopez DG, Vazquez-Victorio G, Rosales-Alvarez RE, Macias-Silva M. Transcriptional cofactors Ski and SnoN are major regulators of the TGF-beta/Smad signaling pathway in health and disease. *Signal Transduct Target Ther*. 2018;3:15.
37. Luo K. Ski and SnoN: negative regulators of TGF-beta signaling. *Curr Opin Genet Dev*. 2004;14:65–70.
38. Bonni S, Wang HR, Causing CG, Kavsak P, Stroschein SL, Luo K, et al. TGF-beta induces assembly of a Smad2-Smurf2 ubiquitin ligase complex that targets SnoN for degradation. *Nat Cell Biol*. 2001;3:587–95.
39. Sun Y, Liu X, Ng-Eaton E, Lodish HF, Weinberg RA. SnoN and Ski proto-oncoproteins are rapidly degraded in response to transforming growth factor beta signaling. *Proc Natl Acad Sci USA*. 1999;96:12442–7.
40. Band AM, Laiho M. SnoN oncoprotein enhances estrogen receptor-alpha transcriptional activity. *Cell Signal*. 2012;24:922–30.
41. Adhikary A, Chakraborty S, Mazumdar M, Ghosh S, Mukherjee S, Manna A, et al. Inhibition of epithelial to mesenchymal transition by E-cadherin up-regulation via repression of slug transcription and inhibition of E-cadherin degradation: dual role of scaffold/matrix attachment region-binding protein 1 (SMAR1) in breast cancer cells. *J Biol Chem*. 2014;289:25431–44.
42. Li Y, Seto E. HDACs and HDAC inhibitors in cancer development and therapy. *Cold Spring Harb Perspect Med*. 2016;6:10.
43. Hu Y, Nie Q, Dai M, Chen F, Wu H. Histone deacetylases inhibit the Snail2-mediated EMT during metastasis of hepatocellular carcinoma cells. *Front Cell Dev Biol*. 2020;8:752.
44. Oliveira T, Hermann E, Lin D, Chowanadisai W, Hull E, Montgomery M. HDAC inhibition induces EMT and alterations in cellular iron homeostasis to augment ferroptosis sensitivity in SW13 cells. *Redox Biol*. 2021;47:102149.
45. Ma C, Huang S, Xu L, Tian L, Yang Y, Wang J. Transcription co-activator P300 activates Elk1-aPKC-iota signaling mediated epithelial-to-mesenchymal transition and malignancy in hepatocellular carcinoma. *Oncogenesis* 2020;9:32.
46. Liao ZW, Zhao L, Cai MY, Xi M, He LR, Yu F, et al. P300 promotes migration, invasion and epithelial-mesenchymal transition in a nasopharyngeal carcinoma cell line. *Oncol Lett*. 2017;13:763–9.
47. Wang J, Wu M, Zheng D, Zhang H, Lv Y, Zhang L, et al. Garcinol inhibits esophageal cancer metastasis by suppressing the p300 and TGF-beta1 signaling pathways. *Acta Pharmacol Sin*. 2020;41:82–92.
48. Fermento ME, Gandini NA, Salomon DG, Ferronato MJ, Vitale CA, Arevalo J, et al. Inhibition of p300 suppresses growth of breast cancer. Role p300 Subcell localization. *Exp Mol Pathol*. 2014;97:411–24.
49. Xiao XS, Cai MY, Chen JW, Guan XY, Kung HF, Zeng YX, et al. High expression of p300 in human breast cancer correlates with tumor recurrence and predicts adverse prognosis. *Chin J Cancer Res = Chung-kuo yen cheng yen chiu*. 2011;23:201–7.
50. Li HM, Bi YR, Li Y, Fu R, Lv WC, Jiang N, et al. A potent CBP/p300-Snail interaction inhibitor suppresses tumor growth and metastasis in wild-type p53-expressing cancer. *Sci Adv*. 2020;6:eaaaw8500.
51. Hsu YH, Sarker KP, Pot I, Chan A, Netherton SJ, Bonni S. Sumoylated SnoN represses transcription in a promoter-specific manner. *J Biol Chem*. 2006;281:33008–18.
52. Nagano Y, Mavrakis KJ, Lee KL, Fujii T, Koinuma D, Sase H, et al. Arkadia induces degradation of SnoN and c-Ski to enhance transforming growth factor-beta signaling. *J Biol Chem*. 2007;282:20492–501.
53. Wan Y, Liu X, Kirschnner MW. The anaphase-promoting complex mediates TGF-beta signaling by targeting SnoN for destruction. *Mol Cell*. 2001;8:1027–39.

ACKNOWLEDGEMENTS

We would like to thank Dr. Derrick Rancourt and Dr. Tannin Schmidt for the use of the Olympus IX70 and the Olympus Fluoview FV1000 fluorescence microscopes, respectively, and Parisa Ghahremanifard for technical assistance. The study was supported by grants from the Natural Sciences and Engineering Research Council of Canada (NSERC), the Canadian Cancer Society (CCS), the Breast Cancer Society of Canada (BCSC), and the Calgary Centre for Cancer Research (CCCR) to S. Bonni, and the National Institutes of Health (NIH) - NS041021 to A. Bonni. A. Chanda is a recipient of a Charbonneau Cancer Institute Director's Award for Excellence in Research Productivity, an Eyes High International Doctoral Scholarship, a William H Davies Medical Research Scholarship, an Achievers in Medical Science (AIMS) Graduate Recruitment Scholarship, and an Eyes High Recruitment Award from the University of Calgary. A. Sarkar is the recipient of an Eyes High Doctoral Recruitment Scholarship and two Alberta Graduate Excellence Scholarships (international), respectively, from the University of Calgary.

AUTHOR CONTRIBUTIONS

Conceptualization: SB, AC, AB. Formal analysis: AC, AS. Funding acquisition: SB, AB. Investigation: AC, AS, LD. Resources: SB. Supervision: SB. Visualization: SB, AC, AS. Writing—original draft: AC, SB, AS, AB. Writing—review & editing: SB, AC, AS, AB, LD.

COMPETING INTERESTS

AB a full-time employee and shareholder of F. Hoffmann-LaRoche Ltd. The study is not funded by F. Hoffmann-LaRoche Ltd. The remaining authors declare no competing interests.

ADDITIONAL INFORMATION

Supplementary information The online version contains supplementary material available at <https://doi.org/10.1038/s41419-023-05921-x>.

Correspondence and requests for materials should be addressed to Shirin Bonni.

Reprints and permission information is available at <http://www.nature.com/reprints>

Publisher's note Springer Nature remains neutral with regard to jurisdictional claims in published maps and institutional affiliations.

Ethics approval and consent to participate: Not applicable.



Open Access This article is licensed under a Creative Commons Attribution 4.0 International License, which permits use, sharing, adaptation, distribution and reproduction in any medium or format, as long as you give appropriate credit to the original author(s) and the source, provide a link to the Creative Commons license, and indicate if changes were made. The images or other third party material in this article are included in the article's Creative Commons license, unless indicated otherwise in a credit line to the material. If material is not included in the article's Creative Commons license and your intended use is not permitted by statutory regulation or exceeds the permitted use, you will need to obtain permission directly from the copyright holder. To view a copy of this license, visit <http://creativecommons.org/licenses/by/4.0/>.

© The Author(s) 2023